Finite-Difference Time-Domain Algorithm for Solving Maxwell's Equations in Rotationally Symmetric Geometries

Yinchao Chen, *Member, IEEE*, Raj Mittra, *Life Fellow, IEEE*, and Paul Harms, *Member, IEEE*

Abstract— **In this paper, an efficient finite-difference time-domain algorithm (FDTD) is presented for solving Maxwell's equations with rotationally symmetric geometries. The azimuthal symmetry enables us to employ a two-dimensional (2-D) difference lattice by projecting the three-dimensional (3-D) Yee-cell in cylindrical coordinates (r, ϕ, z) onto the r-z plane. Extensive numerical results have been derived for various cavity structures and these results have been compared with those available in the literature. Excellent agreement has been observed for all of the cases investigated.**

I. Introduction

THE SOLUTION of Maxwell's equations in the time domain is becoming increasingly important as a tool for analyzing the microwave systems. One of the principle advantages of the time-domain technique is its ability to model the electromagnetic fields in an arbitrary geometry over a broad frequency bandwidth. Since the initial work of Yee [1], the finite-difference time-domain method (FDTD) has been extensively used and developed for electromagnetic computations, and its applications cover many areas in electromagnetics [2]. Rotationally symmetric structures, e.g., the coaxial waveguide and the cylindrical cavity are frequently encountered in microwave engineering, and the objective of this paper is to present an efficient and memory-saving FDTD algorithm for modeling these structures. The nonorthogonal approach such as in [3], [4] can be employed, but it is not efficient for symmetric structures. These structures have been solved in the past with frequency domain approaches such as the finite element method and the finite integration technique, but methods of this type may require the solution of a large sparse matrix equation that is avoided in the time domain approach [5]. By using the recursive algorithm in the time domain, a very large number of unknowns can be readily handled.

Manuscript received April 10, 1995; revised February 15, 1996. This work was supported in part by the Joint Services Electronics Program under Grant N00014-96-1-0129.

Y. Chen is with the Department of Electronic Engineering, Hong Kong Polytechnic University, Hong Kong.

R. Mittra is with the Electromagnetic Communication Laboratory, Department of Electrical and Computer Engineering, University of Illinois at Urbana-Champaign, Urbana, IL USA.

P. Harms is with the Department of Electrical and Computer Engineering University of Kentucky, Lexington, KY USA.

Publisher Item Identifier S 0018-9480(96)03807-0.

II. FDTD Algorithm for Rotationally Symmetrical Structures

A. Assumption for Angular Variation

Instead of using the three-dimensional (3-D) technique described in [2], we introduce a simplified two-dimensional (2-D) FDTD algorithm for rotationally symmetric structures. We begin with the assumption that the angular variation of the electromagnetic fields has either a $\sin(m\phi)$ or $\cos(m\phi)$ variation, and, hence this angular behavior can be factored out from the Maxwell's equations. For generality, we assume that the relative permittivity, permeability, and electric and magnetic conductivities have the biaxial tensor form in cylindrical coordinates given by

$$[\alpha] = \begin{bmatrix} \alpha_r & 0 & 0 \\ 0 & \alpha_\phi & 0 \\ 0 & 0 & \alpha_z \end{bmatrix} \tag{1}$$

where α represents the relative permittivity (ε_r), relative permeability (μ_r), the electric conductivity (σ_e), or the magnetic conductivity (σ_m). Using the generalized differential matrix operators [7], we can express the Maxwell's curl equations as

$$\begin{bmatrix} 0 & -\partial_z & \pm m/r \\ \partial_z & 0 & -\partial_r \\ \mp m/r & (\partial r_r)/r & 0 \end{bmatrix} \begin{bmatrix} E_r \\ E_\phi \\ E_z \end{bmatrix} = -\begin{bmatrix} (\mu_0\mu_r\partial_t + \sigma_{mr})H_r \\ (\mu_0\mu_\phi\partial_t + \sigma_{m\phi})H_\phi \\ (\mu_0\mu_z\partial_t + \sigma_{mz})H_z \end{bmatrix} \tag{2a}$$

$$\begin{bmatrix} 0 & -\partial_z & \mp m/r \\ \partial_z & 0 & -\partial_r \\ \pm m/r & (\partial r_r)/r & 0 \end{bmatrix} \begin{bmatrix} H_r \\ H_\phi \\ H_z \end{bmatrix} = \begin{bmatrix} (\varepsilon_0\varepsilon_r\partial_t + \sigma_{er})E_r \\ (\varepsilon_0\varepsilon_\phi\partial_t + \sigma_{e\phi})E_\phi \\ (\varepsilon_0\varepsilon_z\partial_t + \sigma_{ez})E_z \end{bmatrix} \tag{2b}$$

where ∂_α denotes $\partial/\partial\alpha (\alpha = r, z, t)$. In the following, we let $\sigma_m = 0$ and $\sigma_e = \sigma$ for the sake of simplicity.

B. The 2-D Difference Lattice

It is evident that, in view of (2), the fields at any arbitrary $\phi = \phi_o$ plane can be readily related to its corresponding value in the reference ϕ-plane, *viz.*, $\phi = 0$. This enables us to reduce the original Yee algorithm in 3-D to an equivalent 2-D one,

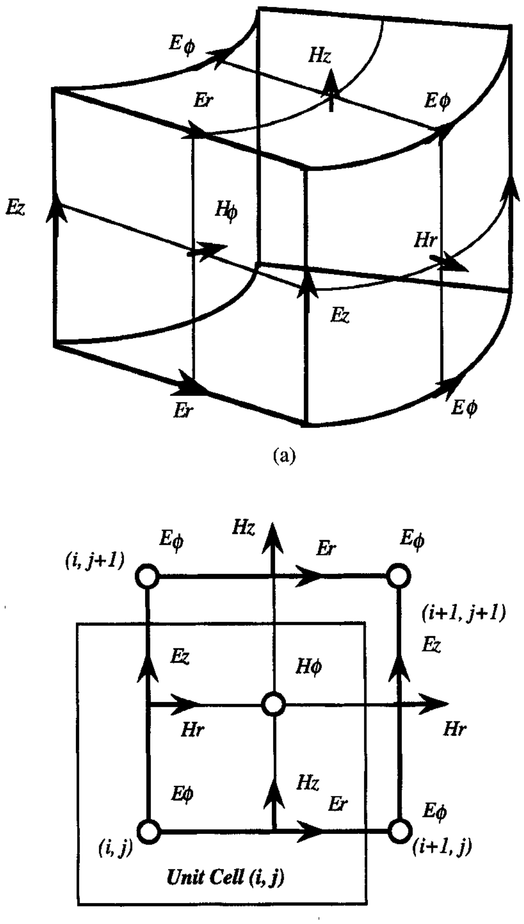

Fig. 1. (a) Conventional 3-D FDTD lattice in cylindrical coordinates. (b) Projection of 3-D FDTD cell at r-z plane.

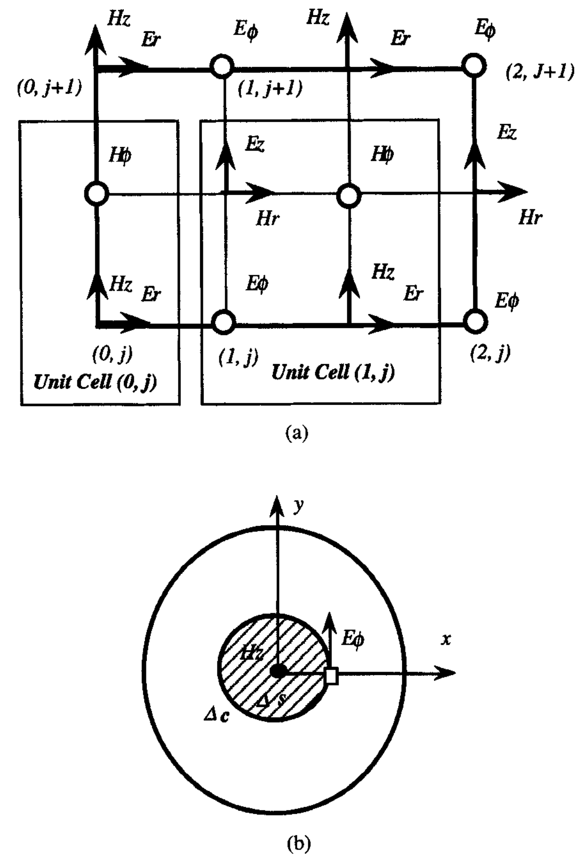

Fig. 2. (a) A portion of the FDTD lattice at $r = 0$. (b) Integral path to evaluate H_z at $r = 0$.

say in the $\phi = 0$ plane. We begin with the 3-D Yee-cell in cylindrical coordinates as shown in Fig. 1(a), and project it onto the r-z plane resulting in the 2-D finite difference lattice shown in Fig. 1(b), which is also similar to the grid in [5].

This 2-D FDTD lattice is different from the conventional 3-D case in the following two ways: i) (E_z, H_r) and (E_r, H_z) share the same geometrical locations; and ii) E_ϕ is located at the four corners of the cell. However, as in the conventional Yee lattice, H_ϕ still resides at the center of the face.

C. Finite-Difference Time-Domain for the Equivalent 2-D Lattice for Cylindrical Systems

Discetizing the two curl equations (2a) and (2b) in the 2-D cell in Fig. 1(b), we obtain

$$
\begin{aligned}
E_r^{n+1}(i,j) &= \frac{\left(1-\dfrac{\sigma_r\Delta t}{2\varepsilon_0\varepsilon_r}\right)}{\left(1+\dfrac{\sigma_r\Delta t}{2\varepsilon_0\varepsilon_r}\right)}E_r^n(i,j) - \frac{\dfrac{\Delta t}{\varepsilon_0\varepsilon_r}}{\left(1+\dfrac{\sigma_r\Delta t}{2\varepsilon_0\varepsilon_r}\right)} \cdot \left[\frac{H_\phi^{n+1/2}(i,j)-H_\phi^{n+1/2}(i,j-1)}{\Delta z}\right] \\
&\quad - \frac{\dfrac{m\Delta t}{\varepsilon_0\varepsilon_r}}{\left(1+\dfrac{\sigma_r\Delta t}{2\varepsilon_0\varepsilon_r}\right)}\frac{H_z^{n+1/2}(i,j)}{r_{i+1/2}}
\end{aligned}
\tag{3a}
$$

$$
\begin{aligned}
E_\phi^{n+1}(i,j) &= \frac{\left(1-\dfrac{\sigma_\phi\Delta t}{2\varepsilon_0\varepsilon_\phi}\right)}{\left(1+\dfrac{\sigma_\phi\Delta t}{2\varepsilon_0\varepsilon_\phi}\right)}E_\phi^n(i,j) + \frac{\dfrac{\Delta t}{\varepsilon_0\varepsilon_\phi}}{\left(1+\dfrac{\sigma_\phi\Delta t}{2\varepsilon_0\varepsilon_\phi}\right)} \cdot \left[\frac{H_r^{n+1/2}(i,j)-H_r^{n+1/2}(i,j-1)}{\Delta z}\right] \\
&\quad - \frac{\dfrac{\Delta t}{\varepsilon_0\varepsilon_\phi}}{\left(1+\dfrac{\sigma_\phi\Delta t}{2\varepsilon_0\varepsilon_\phi}\right)} \cdot \left[\frac{H_z^{n+1/2}(i,j)-H_z^{n+1/2}(i-1,j)}{\Delta r}\right]
\end{aligned}
\tag{3b}
$$

$$
E_z^{n+1}(i,j) = \frac{\left(1-\dfrac{\sigma_z\Delta t}{2\varepsilon_0\varepsilon_z}\right)}{\left(1+\dfrac{\sigma_z\Delta t}{2\varepsilon_0\varepsilon_z}\right)}E_z^n(i,j) + \frac{\dfrac{m\Delta t}{\varepsilon_0\varepsilon_z}}{\left(1+\dfrac{\sigma_z\Delta t}{2\varepsilon_0\varepsilon_z}\right)}
$$

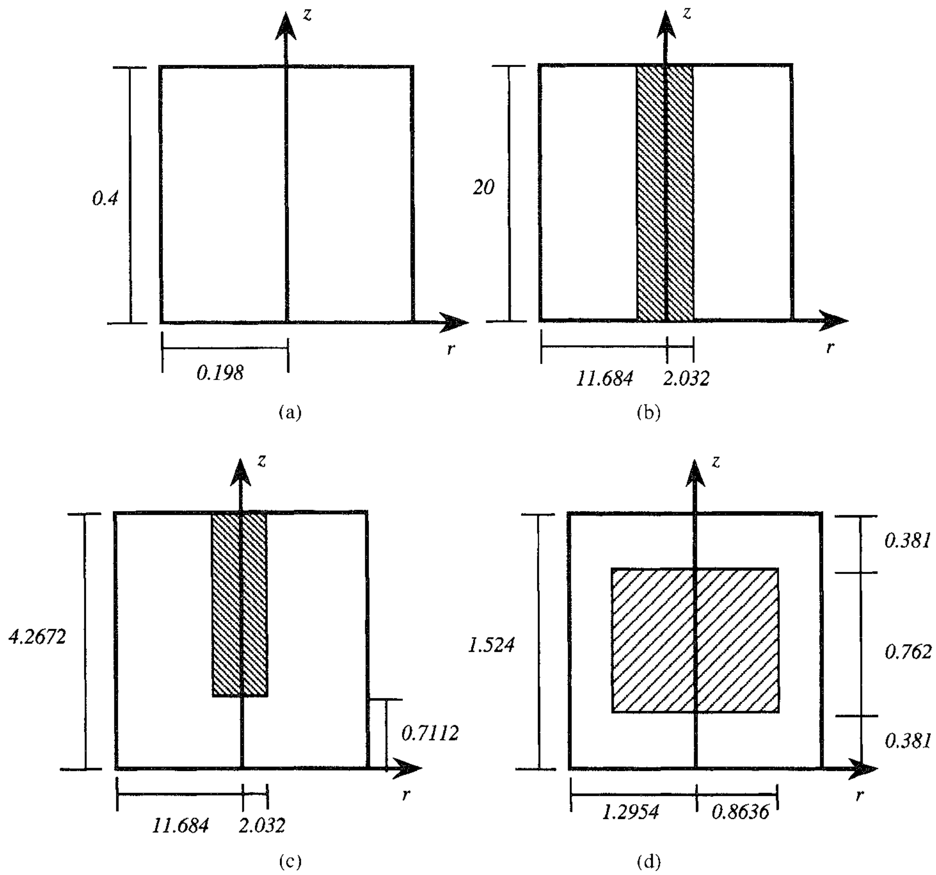

Fig. 3. (a) Cross section of cylindrical cavity (dimension in cm). (b) Cross section of coaxial cavity (dimension in cm). (c) Cross section of capacitively-loaded cavity (dimension in cm). (d) Cross section of cylindrical cavity with a dielectric disk filling ($\varepsilon_r = 35.74$ and dimension in cm). (e) Cross section of loaded cavity with an inner conductor of complex shape (dimension in cm).

$$\cdot \frac{H_r^{n+1/2}(i,j)}{r_i} + \frac{\dfrac{\Delta t}{\varepsilon_0\varepsilon_z}}{\left(1+\dfrac{\sigma_z \Delta t}{2\varepsilon_0\varepsilon_z}\right)} \cdot \left[\frac{r_{i+1/2}H_\phi^{n+1/2}(i,j) - r_{i-1/2}H_\phi^{n+1/2}(i-1,j)}{r_i \Delta r}\right] \tag{3c}$$

$$H_r^{n+1/2}(i,j) = H_r^{n-1/2}(i,j) - \frac{m\Delta t}{\mu_0\mu_r r_i}E_z^n(i,j) + \frac{\Delta t}{\mu_0\mu_r}\left[\frac{E_\phi^n(i,j+1) - E_\phi^n(i,j)}{\Delta z}\right] \tag{4a}$$

$$H_\phi^{n+1/2}(i,j) = H_\phi^{n-1/2}(i,j) - \frac{\Delta t}{\mu_0\mu_\phi} \cdot \left[\frac{E_r^n(i,j+1) - E_r^n(i,j)}{\Delta z} - \frac{E_z^n(i+1,j) - E_z^n(i,j)}{\Delta r}\right] \tag{4b}$$

$$H_z^{n+1/2}(i,j) = H_z^{n-1/2}(i,j) + \frac{m\Delta t}{\mu_0\mu_z r_{i+1/2}}E_r^n(i,j) - \frac{\Delta t}{\mu_0\mu_z}\left[\frac{r_{i+1}E_\phi^n(i+1,j) - r_i E_\phi^n(i,j)}{r_{i+1/2}\Delta r}\right] \tag{4c}$$

where $r_i = (i - 1/2)\Delta r$ and $r_{1/2} = r_0 = 0$, and the fields associated with coordinate (i,j) are enclosed with the box shown in Fig. 1(b).

The above equations, which include the appropriate metric coefficients in the cylindrical coordinates, are suitable for the time domain iteration once the problem of singularities and of these coefficients at $r = 0$ in (3a), (3c), and (4c) has been addressed. This is discussed in the following section.

D. Handling the Singularities at $r = 0$

The electromagnetic fields E_r, H_ϕ, and H_z at one of the natural boundaries of the computational domain in the $\phi = 0$ plane, *viz.*, the cylindrical axis ($r = 0$), must be uniquely defined. Even though E_r, H_ϕ and H_z exhibit singularities at $r = 0$, the actual fields there must be finite in both the time and frequency domains. Hence, these singularities must be removed before (3) and (4) could be used for time stepping. To this end, we consider a portion of the FDTD lattice at $r = 0$, as shown in Fig. 2(a). In this figure i is the lattice index for the radial dimension, and j is the lattice index for the axial dimension.

On the natural boundary, $r = 0$, there exists a total of three components, *viz.*, E_r, H_ϕ and H_z. However, as seen from (3b) and (3c), only the components tangential to this boundary, *i.e.*, H_ϕ and H_z, are needed to update the adjacent E_ϕ and E_z fields internal to the mesh. We note from (3c) that to compute E_z at

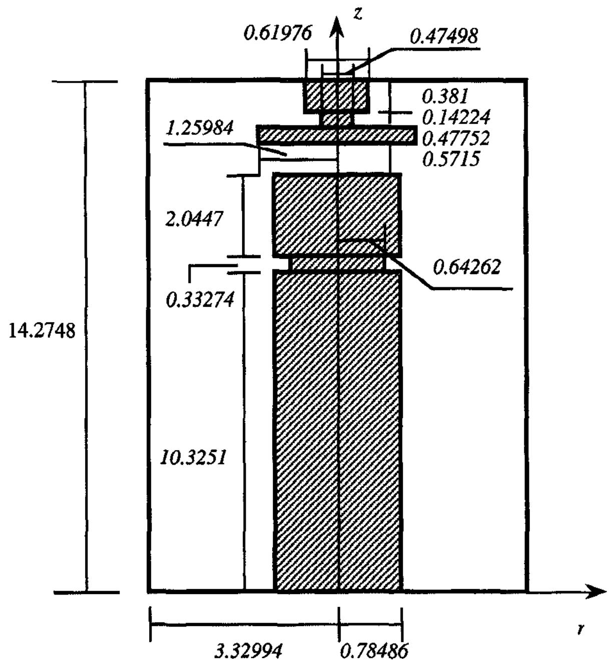

(e)

Fig. 3. (Continued)

TABLE I
RESONANT FREQUENCIES FOR TE_z AND TM_z MODE (GHz)

Mode	010	011	012	013	014	015	020	021	022	023
TE_z		0.997	1.189	1.455	1.761			1.732	1.849	
TM_z	0.579	0.690	0.947	1.265	1.601	1.961	1.330	1.382	1.527	1.742

$i = 1, H_\phi$ at $i = 0$ is to be multiplied by a factor $r_{i-1/2}$ which is zero since $r_{i-1/2} = r_{1/2} = 0$, hence, H_ϕ at $r = 0$ is not needed. We further note that from (3b) to compute E_ϕ at $i = 1$ we need to know H_z at $i = 0$. In summary, only H_z is needed at the boundary $i = 0$ to update all of the relevant fields.

From (2b), we note that H_z is zero at $r = 0$ for $m \neq 0$; hence, we only need to evaluate H_z at $r = 0$ for $m = 0$. To this end, we start from the integral form of Maxwell's equation in the time domain, *viz.*

$$\oint_{\Delta c} \vec{E} \cdot d\vec{l} = -\iint_{\Delta s} \mu \frac{\partial \vec{H}}{\partial t} \cdot d\vec{s} \tag{5}$$

where Δs and Δc are the finite difference area and integral paths defined in Fig. 2(b). From (5), we can obtain the following time update equation for H_z at $r = 0$ and $m = 0$

$$H_z^{n+1/2}(0, j) = H_z^{n-1/2}(0, j) - \frac{4\Delta t}{\mu_0 \mu_z \Delta r} E_\phi^n(1, j). \tag{6}$$

Once H_z is known at $r = 0$ the rest of the field components can be evaluated using (3) and (4).

E. Numerical Implementation of Blackman–Harris Windows Excitation

To suppress the initial transients, the Blackman–Harris (BH) window function has been used in this work instead of the Gaussian excitation function [8]. Since the sidelobe level of the window function is approximately −92 dB, the BH window function provides a smoother transition of the excitation function. The BH function is discretized in the following form as shown in (7) at the bottom of the page, where t_n is the time step, t_c indicates the time position for

$$w(t_n) = \begin{cases} \left\{ \begin{aligned} &0.35875 + 0.48829 \cos\left(\frac{\pi(t_n - t_c)}{N_{\text{half}}}\right) \\ &\quad +0.14128 \cos\left(\frac{2\pi(t_n - t_c)}{N_{\text{half}}}\right) + 0.01168 \cos\left(\frac{3\pi(t_n - t_c)}{N_{\text{half}}}\right) \end{aligned} \right\} & t_n \in [t_c - N_{\text{half}}, t_c + N_{\text{half}}] \\ 0, & \text{otherwise} \end{cases} \tag{7}$$

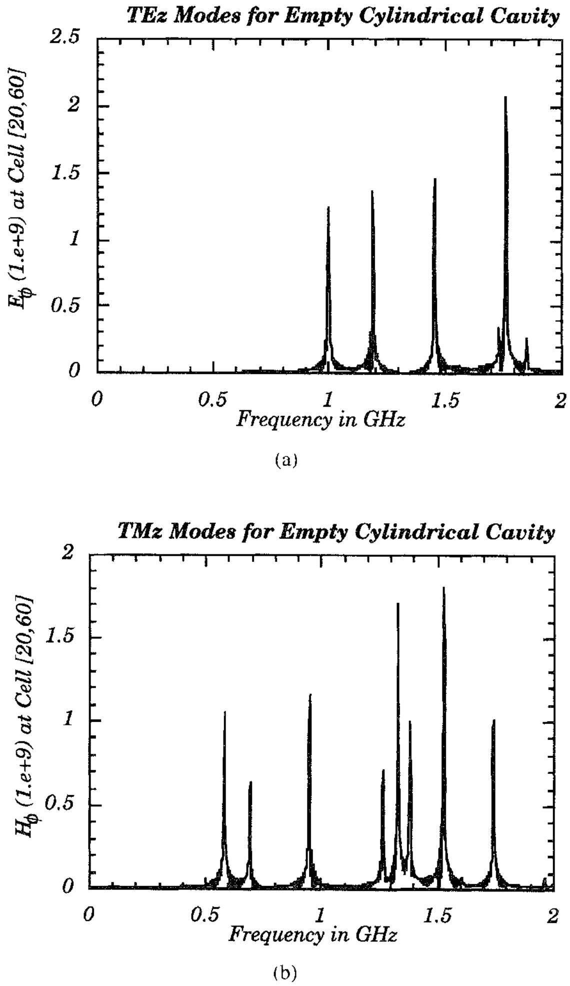

Fig. 4. (a) E_ϕ at cell [20, 60] as a function of frequency for an empty cylindrical cavity. (b) H_ϕ at cell [20, 60] as a function of frequency for an empty cylindrical cavity.

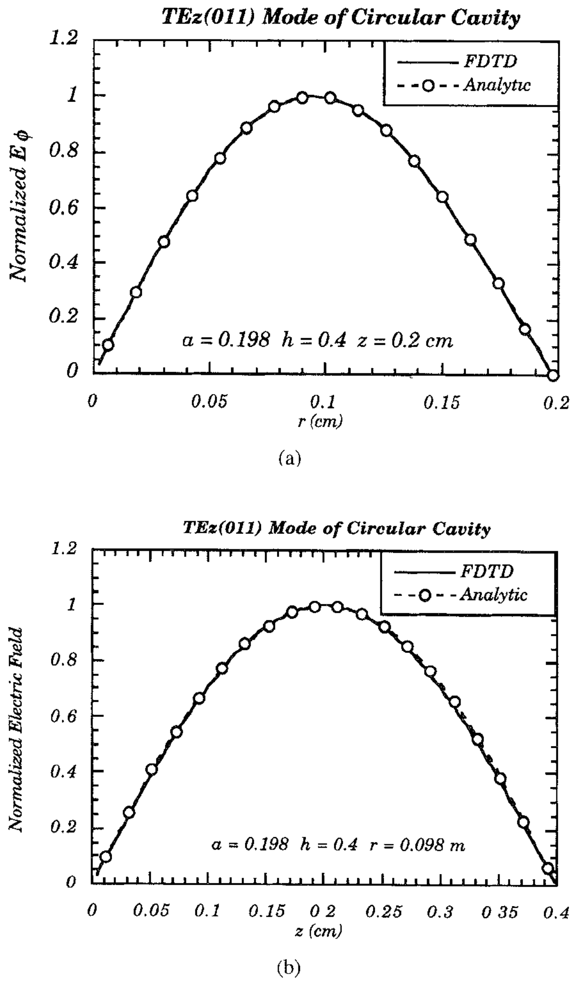

Fig. 5. (a) Normalized distribution of E_ϕ along the radius at $z = 0.2$ cm for TE_{z011} mode. (b) Normalized distribution of E_ϕ along the height at $r = 0.098$ cm for TE_{z011} mode.

the center of the window function, and N_{half} is the designed half width of the BH window function. It is evident from (7) that the BH window function is turned on only during a designed time interval. In practice, a small value of N_{half} is chosen to obtain a broad frequency band, and a large value is chosen when the desired bandwidth is narrow. In this work, the window function is implemented as a soft source for exciting both TM_ϕ and TE_ϕ modes.

It is implied that rotationally symmetric excitations are automatically taken even though the sources are located on the r-z plane in the practical computations.

III. Numerical Results

We have investigated the resonant properties of a number of cylindrical cavities, shown in Fig. 3, by using the rotationally symmetric FDTD algorithm described in the last section. To construct the FDTD grids for these geometries, a mesh generator has been developed to provide the geometrical and material input files to the FDTD solver.

A. Empty Cylindrical Cavity

A cross section of the empty cylindrical cavity and its dimensions are shown Fig. 3(a), which was discretized by using 50 by 100 cells along r and z, respectively. The analytical resonant frequencies [9] for both the TE_z and TM_z modes are listed in Table I. In Fig. 4(a) and (b), we display a frequency spectrum of the field components E_ϕ and H_ϕ at cell [20, 60] for the TE_z and TM_z modes, respectively. Table I shows excellent agreement between the computed and analytical resonant frequencies for the dominant mode and the higher-order modes, and the relative error is seen to be less than 0.5%. Fig. 5(a) and (b) show that the normalized electric field E_ϕ along the two center cuts for the TE_{z011} mode compares very well with the analytical results.

B. Coaxial Cavity

The next geometry investigated was that shown in Fig. 3(b) of the coaxial cavity. The FDTD result for the dominant mode was compared with that given in Marcuvitz [10], which predicted a resonant frequency of 1.5027 GHz. Fig. 6 shows the FDTD results for H_ϕ at cell [20, 60] in the entire frequency range from 0 to 3 GHz. The dominant resonant frequency (DRF) computed by the FDTD method was 1.5075 GHz. The approximate procedure of Marcuvitz [10] is valid only for the

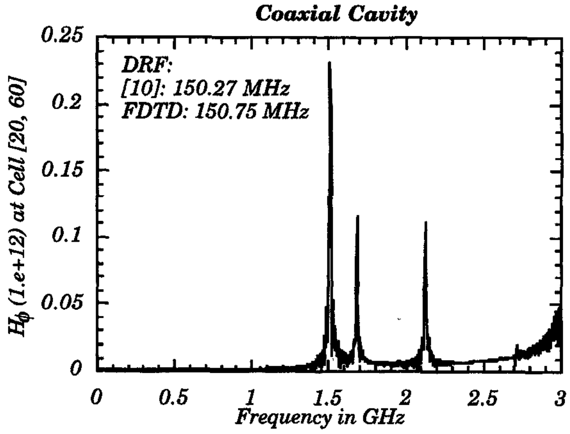

Fig. 6. H_ϕ at cell [20, 60] as a function of frequency for a coaxial cavity.

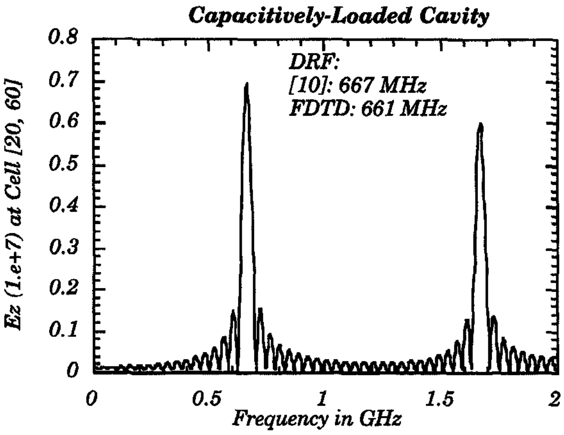

Fig. 7. E_z at cell [20, 60] as a function of frequency for a capacitively-loaded cavity.

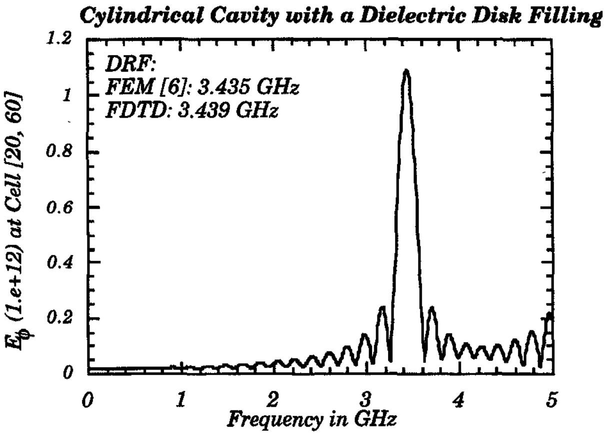

Fig. 8. E_ϕ at cell [20, 60] as a function of frequency for a cylindrical cavity with a dielectric disk filling.

dominant mode, hence, it was not possible to compare the results for the higher-order modes with those based on the Marcuvitz method.

C. Capacitively-Loaded Cavity

Another interesting structure is the capacitively-loaded cavity shown in Fig. 3(c). It is similar to the coaxial geometry, but its inner conductor only makes contact with the top wall. The dominant resonant frequency of 0.661 GHz derived by using the FDTD method, and shown in Fig. 7, agrees well with the resonant frequency of 0.667 GHz computed with the approximate method [10].

D. Cylindrical Cavity with a Dielectric Disk Filling

In microwave applications, cavities filled with dielectric material are used quite extensively. We consider the case of a dielectric disk located in the center of a cylindrical cavity, as shown Fig. 3(d). The finite element analysis yielded the resonant frequency of 3.435 GHz for the TE_{01} mode [3], which compares well with the FDTD result of 3.439 GHz, shown in Fig. 8. The distributions of E_r, E_ϕ and H_z fields at the dominant resonant frequency are displayed in Fig. 9(a), (b), and (c). The dimensions in these figures are in meters. It is evident that the electromagnetic energy in this cavity is concentrated either inside or in the vicinity of the dielectric disk.

E. Loaded Cavity with an Inner Conductor of Complex Shape

For the final example, we analyze a cavity structure whose inner conductor has a complex configuration, as shown in Fig. 3(e). The computed resonant frequency for the dominant mode, plotted in Fig. 10, is 500.63 MHz, and it compares well with the measured data of 501 MHz, despite the fact that the physical cavity structure is slightly asymmetric due to the presence of the feed and coupling ports.

IV. Conclusion

An efficient FDTD algorithm for solving Maxwell's equations for rotationally symmetric structures has been presented. A number of representative cylindrical cavities have been investigated, and the algorithm has been validated by comparing

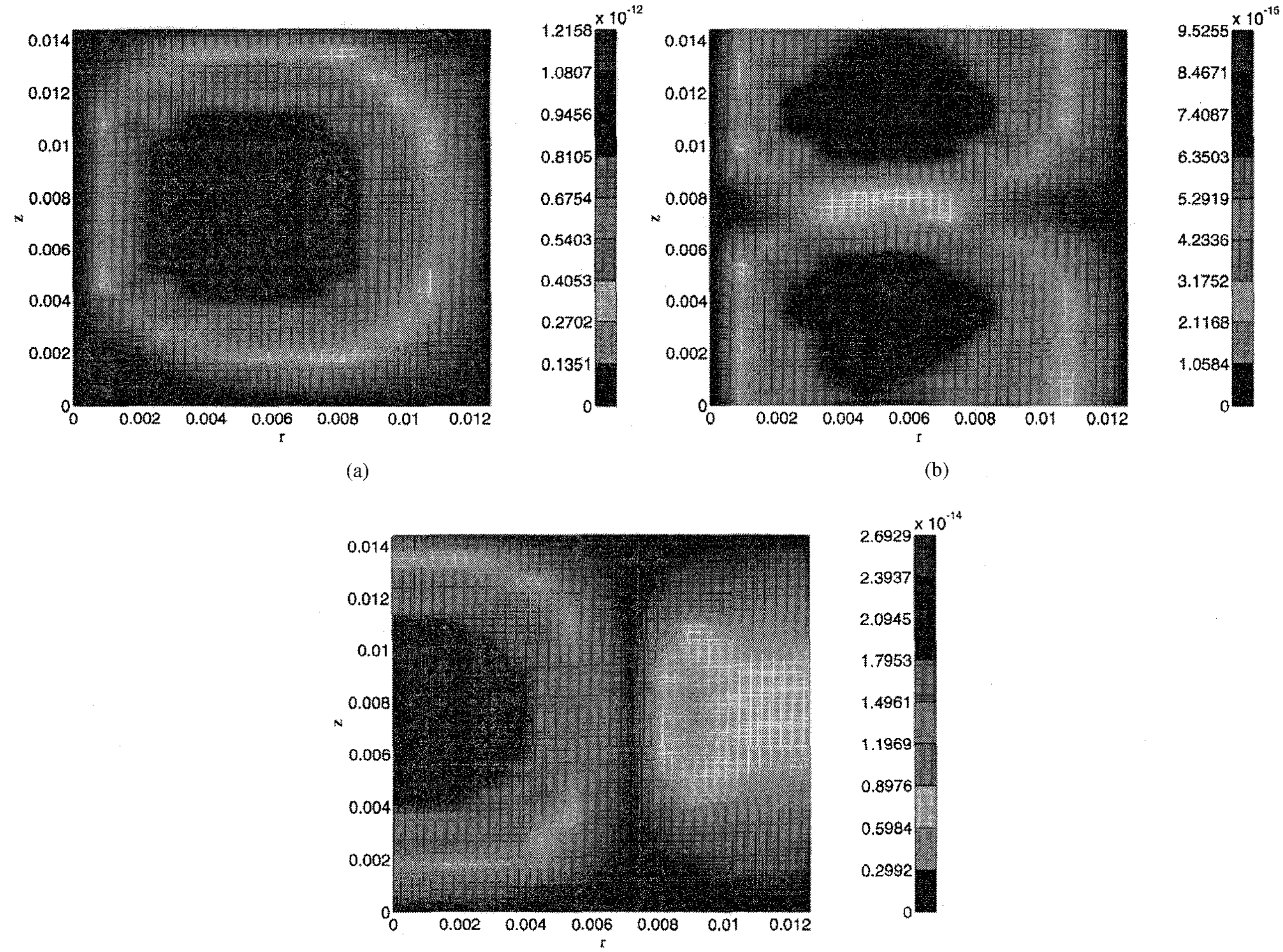

Fig. 9. (a) Distribution of E_ϕ in the right half of the cylindrical cavity with a dielectric disk filling. (b) Distribution of H_r in the right half of the cylindrical cavity with a dielectric disk filling. (c) Distribution of H_z in the right half of the cylindrical cavity with a dielectric disk filling.

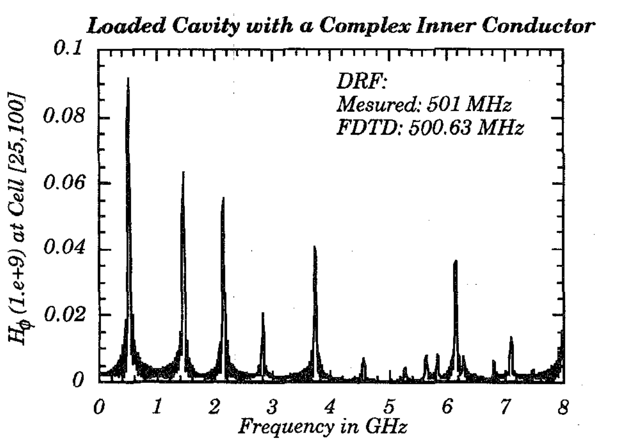

Fig. 10. H_ϕ at cell [25, 100] as a function of frequency for a loaded cavity with an inner conductor of complex shape.

its results with the analytical, numerical and experiment results published elsewhere.

ACKNOWLEDGMENT

The authors would like to thank S. Kosanovich, formerly of the University of Illinois at Urbana-Champaign, for his valuable suggestions and discussions.

REFERENCES

[1] K. S. Yee, "Numerical solution of initial boundary value problems involving Maxwell's equations in isotropic media," *IEEE Trans. Antenna Propagat.*, vol. AP-14, pp. 302–307, May 1966.

[2] K. S. Kunz and R. J. Luebbers, *The Finite Difference Time Domain Method for Electromagnetics.* Boca Raton, FL: CRC Press, 1993.

[3] P. H. Harms, J. F. Lee, and R. Mittra, "A study of the nonorthogonal FDTD method versus the conventional FDTD technique for computing resonant frequencies of cylindrical cavities," *IEEE Trans. Microwave Theory Tech.*, vol. 40, pp. 741–746, Apr. 1992.

[4] ——, "Corrections to 'A study of the nonorthogonal FDTD method versus the conventional FDTD technique for computing resonant frequencies of cylindrical cavities'," *IEEE Trans. Microwave Theory Tech.*, vol. 40, pp. 2115–2116, Nov. 1992.

[5] J. E. Lebaric and D. Kajfez, "Analysis of dielectric resonator cavities using the finite integration technique," *IEEE Trans. Microwave Theory Tech.*, vol. 37, pp. 1740–1748, Nov. 1989.

[6] M. M. Taheri and D. Mirshekar-syahkal, "Accurate determination of modes in dielectric-loaded cylindrical cavities using a one-dimensional finite element method," *IEEE Trans. Microwave Theory Tech.*, vol. 37, pp. 1536–1541, Oct. 1989.

[7] Y. Chen, K. Sun, B. Beker, and R. Mittra, "Unified matrix presentation of Maxwell's and wave equations using generalized differential matrix operators," submitted to *IEEE Trans. Educ.*

[8] F. J. Harris, "On the use of windows for harmonic analysis with discrete Fourier transform," Proc. *IEEE*, vol. 66, pp. 51–83, Jan. 1978.

[9] C. A. Balanis, *Advanced Engineering Electromagnetics.* New York: Wiley, 1989.

[10] N. Marcuvitz, "Radial transmission lines," in *Principles of Microwave Circuits,* C. G. Montgomery, R. H. Dicke, and E. M. Purcel, Eds. New York: McGraw-Hill, 1948.

Yinchao Chen (M'94) received the Ph.D. degree in electrical engineering from the University of South Carolina, Columbia, SC, in 1992.

From 1989 to 1995, he was a Research Assistant, Postdoctoral Fellow, Adjunct Assistant Professor, and Visiting Scholar Fellow with the University of South Carolina, South Carolina State University, and University of Illinois at Urbana-Champaign, USA, respectively. During his earlier career in China, he was a Microwave and Antenna Engineer with Nanjing Research Institute of Electronic Technology. Currently, he is an Assistant Professor in the Department of Electronic Engineering, Hong Kong Polytechnic University, Hong Kong. His current research interests include computational electromagnetics using various analytical and numerical methods with applications in the areas of millimeter-wave integrated circuits, electronic packaging modeling for VLSI and devices, guided-wave propagation, and antenna engineering. He has published over 40 papers in refereed journals and international symposiums.

Raj Mittra (S'54–M'57–SM'69–F'71–LF'95) is the Director of the Electromagnetic Communication Laboratory of the Electrical and Computer Engineering Department and Research Professor of the Coordinated Science Laboratory at the University of Illinois. He was a Visiting Professor at Oxford University, Oxford, England and at the Technical University of Denmark, Lyngby, Denmark. He is President of RM Associates, which is a consulting organization providing services to serval industrial and governmental organizations, both in the U.S. and abroad. His professional interests include the areas of electromagnetic modeling and simulation of electronic packages, communication antenna design including GPS, broadband antennas, EMC analysis, radar scattering, frequency selective surfaces, microwave and millimeter wave integrated circuits, and satellite antennas. He has published approximately 400 journal papers and 20 books or book chapters on various topics related to electromagnetics.

He is a Life Fellow of the IEEE, a Past-President of AP-S, and has served as the editor of the TRANSACTIONS OF ANTENNAS AND PROPAGATION Society. He won the Guggenheim Fellowship Award in 1965 and the IEEE Centennial Medal in 1984. Currently, he serves as the North American editor of the journal AEÜ.

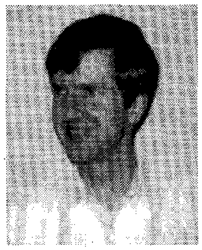

Paul Harms (M'92) received the Ph.D. degree in electrical engineering from the University of Illinois at Urbana-Champaign in 1992. Currently, he is a postdoctoral scholar at the University of Kentucky.

He worked for three years as a postdoctoral Fellow/Consultant at the University of Illinois. His interests are in applied computational and experimental electromagnetics.